Journal of Alloys and Compounds 502 (2010) 16–23

Contents lists available at ScienceDirect

Journal of Alloys and Compounds

journal homepage: www.elsevier.com/locate/jallcom

The single crystal superconducting Bi-2212 whiskers fabrication and their thermal transport properties

S. Altın, M.A. Aksan*, M.E. Yakıncı, Y. Balcı

Inonu Universitesi, Fen Edebiyat Fakultesi, Fizik Bolumu, 44280 Malatya, Turkey

ARTICLE INFO

Article history:
Received 25 December 2009
Received in revised form 9 April 2010
Accepted 23 April 2010
Available online 4 May 2010

PACS:
68.70.+w
74.72.Hs
65.60.+a
74.25.Fy
72.20.Pa

Keywords:
Whiskers
Bi-based cuprates
Thermal properties of glasses
Transport properties (electric and thermal conductivity, thermoelectric effects)

ABSTRACT

In this study, we have fabricated the superconducting single crystal whiskers using glass–ceramic BiSrCaCuO material. The crystallization kinetic studies (crystallization activation energy, E_a, and the Avrami parameter, n,) were carried out using DTA data. The oxygen diffusion energy was calculated using TG data. XRD and SEM analysis of the whiskers showed Bi-2212 phase formation and the c-axis orientation. The in-plane resistivity, ρ_{ab}, and the out-of-plane resistivity, ρ_c, properties of the whiskers were investigated. The thermoelectric power, $S(T)$, value between 10 and 300 K is found to be positive, indicating that charge carriers in the whiskers are holes. We analyzed the thermoelectric power as a function of temperature with "*Two band model with linear T-term*" Linear temperature dependence in the thermal conductivity down to T_c and then a sharp rise just below T_c were obtained.

1. Introduction

High temperature (HT_c) superconducting whiskers due to their single crystal nature are suitable materials for nano/micro scale technological applications such as Josephson Junctions [1,2] and terahertz frequency generators/oscillators using Josephson Plasma properties [3]. They have also significant potential to use as SQUID or microwave radiation detectors and high speed switching gates [4–5].

Different growth techniques such as direct growth from stoichiometric powder/pellet samples by controlled heating or using a flux agent both in the powder or glass precursors have been used to fabricate the BSCCO (Bi-2212) whiskers [6,7–10]. Although whisker growth is observed in all the fabrication techniques, the longest single crystal whiskers (~20 mm long 100–200 μm wide and 50–900 nm thick materials) can be obtained only by glass precursor method, compared to other fabrication techniques. In addition, starting compositions in other fabrication techniques include some doping/substitution elements which act as catalytic impurities [6]. However, catalytic impurities are not necessary for whisker growth in glass precursor method. The Bi-2212 whiskers, obtained by glass precursor method, show the T_c value between 80 and 95 K and the critical current density, J_c, value of $\sim 7 \times 10^6$ A/cm^2 [10–14]. Different elements have been substituted and/or doped to investigate the superconducting properties and growth of whiskers [15–20]. In these studies, it was found that some substitutions/dopings positively influenced the whisker growth but in high substitution/doping levels, relatively small in size and impurity contained whiskers and bad superconducting properties were obtained.

Determination of the conduction mechanism in HT_c superconductors is important to understand transport properties. Thermoelectric power (TEP), S, gives very important information about the nature of the carriers responsible for conduction process, the scattering mechanism and also the band structure of the material. Since the discovery of the HT_c superconductors, many experimental and theoretical studies have been made to evaluate the thermoelectric power data of these cuprates [21–25]. In these studies, it was seen that the variation of thermoelectric power with temperature and hole concentration, p, exhibits common behavior; for the underdoped systems (low carrier concentration) thermoelectric power has positive sign and large. It shows temperature-independent nature particularly at high tem-

* Corresponding author.
E-mail address: maksan@inonu.edu.tr (M.A. Aksan).

0925-8388/$ – see front matter © 2010 Elsevier B.V. All rights reserved.
doi:10.1016/j.jallcom.2010.04.153

Table 1
Summary of the growth conditions of the whiskers.

Heating rate (°C min^{-1})	Cooling rate (°C min^{-1})	Heat treatment conditions		Whiskers length	EDX results of whiskers fabricated
		Temperature (°C)	Time (h)		Bi–Sr–Ca–Cu–Al
10	1	790–805	5–240	Not observed	–
10	1	810	5–240	~80–1.1 mm	29.6–19.2–22.3–28.1–0.8
10	1	820	5–240	~0.5–12 mm	29.1–19.4–22.1–27.3–0.6
10	1	830	5–110	~1.0–3.0 mm	28.7–18.9–21.3–30.2–0.9
10	1	830	5–240	~2.0–4.0 mm	28.8–20.4–22.1–28.2–0.5
10	1	840	5–110	~1.5–8.0 mm	27.3–21.4–21.4–29.1–0.8
10	1	840	5–240	~3.6–13.8 mm	29.4–21.8–20.7–27.5–0.6
10	1	850	5–240	~4.0–18 mm	29.4–19.4–22.1–28.1–0.7
10	1	860	5–120	Not observed	–

peratures. In the overdoped systems (high carrier concentration), thermoelectric power is negative and small, varying almost linearly with temperature. For the optimum doped systems, thermoelectric power first increases with temperature and reaches a maximum at around T_c and then decreases [26].

Low dimensional materials such as supperlattice structures, quantum wires, single crystals show interesting thermoelectric power behavior. Generally, they display high S value [27].

Thermal conductivity, $\kappa(T)$, measurement is among the transport investigations performed to understand the scattering mechanism of charge carriers, electron–phonon interaction and phonon mean free path in solids. One of the common feature appeared in HT_c superconductivity is the anomalous and sharp rise of $\kappa(T)$ just below the superconducting transition temperature, T_c [28–33]. Two explanations have been suggested for this sharp rise in $\kappa(T)$. One attributes it to a decrease in scattering of phonons by carriers as they condense in the superconducting state [34]. The other attributes it to a decrease in quasi-particle scattering below T_c [35]. Experimental investigations such as microwave conductivity, Thermal Hall Effect measurements support to be the increase in the electronic component around T_c [36–38].

In the present study, we have successfully fabricated Bi-2212 whiskers by glass precursor method. The structural, thermal, crystallization kinetics, electrical properties were investigated. Essentially, transport properties including thermoelectric power and thermal conductivity were extensively studied in this paper.

2. Experimental details

Appropriate amounts of reagent grade Bi_2O_3, $SrCO_3$, $CaCO_3$ and CuO were mixed in agate mortar for 2 h to give a nominal composition of $Bi_3Sr_2Ca_2Cu_3O_{10+\delta}$. The mixtures were melted in an α-Al_2O_3 crucibles at 1150 °C for 3 h. Molten material was then quenched between two cold copper plates. Thus, rapidly quenched, pore-free, and approximately 1.5 mm thick amorphous plates were obtained.

Whiskers were then grown by heating the glass plates in air in a P.I.D. controlled tube furnace. Heat treatments at different temperatures and durations were applied to the glass sample to investigate the whisker growth. The best whisker growth was obtained at 850 °C for 120 h, Table 1.

DTA measurements were carried out based on non-isothermal kinetic theory under O_2 flow up to 900 °C at four different heating rates (5, 10, 15 and 20 °C min^{-1}). Shimatzu system 60 was used for DTA analyses. The crystallization activation energy, E_a, and the Avrami parameter, n, were calculated using Kissinger method and the Ozawa's equation, respectively. Shimatzu system 50 was used for obtaining thermogravimetric (TG) scans. 20 mg grounded glass material was heated at a constant heating rate of 10 °C min^{-1} up to 900 °C under oxygen atmosphere. Mass gain and loss of the material were measured as a function of temperature. Activation energy for oxygen diffusion was calculated using TG data.

Phase identification and crystal structure of the glass material and whisker fabricated were carried out by XRD (Rigaku RadB X-ray diffractometer) using CuKα radiation (λ = 1.5405 Å) between 2θ = 3° and 60° at the scan rate of 3° min^{-1}. 24 μm thick, 2.3 μm width 18 mm length whisker (largest whisker) was used for XRD analysis.

The surface morphology and elemental analysis of the materials during heat treatment were performed in scanning electron microscope (Leo EVO 40XVP) using energy dispersive X-ray spectrometer (Bruker-EDX system).

The temperature dependence of the in-plane resistivity and out-of-plane resistivity was carried out for the whisker fabricated at 850 °C for 120 h. Longest and widest whisker (24 μm thick, 2.3 μm width 18 mm) was used for resistivity measurements. The whisker was cut into two parts: first part is used for in-plane resistivity measurement and the second one for out-of-plane measurement. a-(b-) and c-axis resistivity measurement was performed by contacting with silver and gold deposition as described in Ref. [39]. The T_c value was determined by the resistivity differentiation $d\rho(T)/dT$. The peak temperature in $d\rho(T)/dT$ plot is defined as the T_c value.

Fully automated Quantum Design XL7 PPMS was used during the resistivity measurements. Constant 100 μA current has been applied during the measurements.

Thermoelectric power was measured in the temperature range 10–300 K using the closed cycled refrigerator. Thermoelectric power measurement was carried out only along a(-b) axis, since constant temperature gradient was not established along c-axis due to very short c-axis length (~2 μm). The whisker was clamped between two thin copper plates. Voltages were recorded using Keithley 182 nanovoltmeter. One of the copper plates was placed on the cold head of the system and the other on the hotter head. A temperature gradient of 1 K was established along the sample and determined using a pair of silicon diode. For any temperature, the voltage difference (ΔV) between two terminals was recorded to calculate the TEP value ($S = \Delta V/\Delta T$).

The thermal conductivity was measured using the steady-state heat flow method in the closed cycle refrigerator system. Thermal conductivity measurement was carried out in a(b-) axis of the whisker fabricated at 850 °C for 120 h. The whisker was vertically attached to the system to establish a temperature gradient between bottom and upper ends of the whisker. Bottom end of the whisker was fixed to the cold head of the cryostat system and upper end of the whisker was attached to a heater (25 Ω) which had an indium sheated surface. The sample temperature and temperature gradient across the sample were determined by two silicon thermocouples.

3. Results and discussion

3.1. Thermal analysis results

Fig. 1 shows the DTA curves of the glass Bi-3223 material taken at different heating rates, α. The obtained DTA data are listed in Table 2. The glass transition temperatures, T_g, of the Bi-3223 glass sample were found between 456 and 470 °C, while the first exothermic activity, T_{x1}, was found between 461 and 480 °C, depending on the heating rate, α, Fig. 1. We believe that the T_{x1} temperature

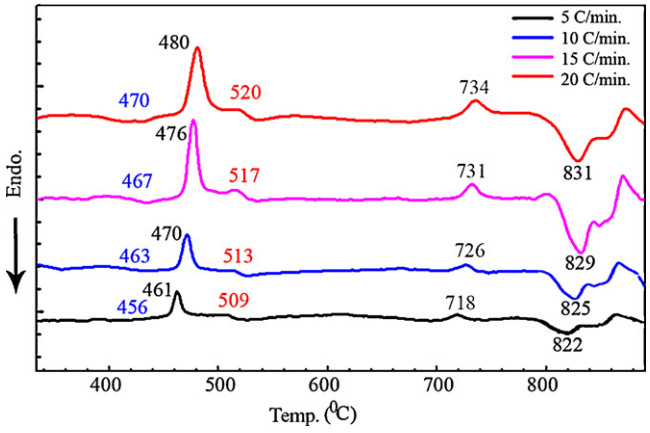

Fig. 1. DTA patterns of the Bi-3223 material at different heating rates.

Table 2
DTA data and activation energy and avrami parameter of Bi-3223 composition.

Heating rate (°C min^{-1})	T_g (°C)	T_{x1} (°C)	ΔT (T_{x1}–T_g) (°C)	T_{x2} (°C)	T_{x3} (°C)	T_{pm} (°C)	E_a (kJ mol^{-1})	n
5	456	461	5	509	718	822	340	2.9 ± 0.3
10	463	470	7	513	726	825		
15	467	476	9	517	731	829		
20	470	480	10	520	734	831		

corresponds to nucleation assisted first crystallization temperature of the BSCCO material. The atomic percentage of the nucleation centres is given in the SEM analysis. The first peak temperature, T_{x1}, however, shifts to the higher temperatures by increasing the heating rate and it is believed that this is highly related with the nucleation rates of the glass material [40,41]. The exothermic peaks between 509 and 520 °C are attributed to the crystallization of the solid solution impurity phases such as Bi-2201, $Sr_3Bi_2Cu_2O_8$ and $(Sr,Ca)_{12}Cu_{24}AlO_x$ which were obtained in XRD analysis.

The third exothermic activity, T_{x3}, obtained between the 718 and 734 °C, corresponded to the formation temperature of the Bi-2201 phase. The endothermic activities between 822 and 831 °C, depending on the heating rate, α, are believed to be due to the formation of the Bi-2212 phase and so the whiskers. The melting temperatures of the sample were obtained after 900 °C depending on the heating rates.

The crystallization kinetics of the Bi-3223 material were carried out using DTA data taken at four uniform heating rates and non-isothermal kinetic model of Kissinger [42]. The Kissinger model, later modified by Matusita and Sakka [43], is also known as an extension of the John-Mehl-Avrami model [44], as expressed by

$$\frac{d\ \ln(\alpha/T_x^2)}{d(1/T_x)} = -\frac{E_a}{R} + \text{Constant} \quad (1)$$

where T_x is the first crystallization temperature, α is the heating rate, E_a is the crystallization activation energy and R is the gas constant. Fig. 2 shows the Kissinger plot for the crystal growth of the sample prepared. If the crystallization mechanism is known and remains constant with the heating rate, the plot of $\ln(\alpha/(T_x)^2)$ vs $1/T_x$ gives the activation energy for crystallization. The calculated E_a value was found to be 340 kJ mol^{-1}. This is in good agreement with the E_a values obtained previously by other research groups for Bi-based materials [45–47].

The Avrami parameter, n, which gives important information about the morphology of the crystal and also crystal growth in the samples, can be calculated from the DTA data [47]:

$$n = \frac{2.5}{\Delta T_{FWHM}} \frac{T_x^2}{E_a/R} \quad (2)$$

where ΔT_{FWHM} is the width of the crystallization peak at half-maximum, T_x is the temperature of the first crystallization peak, E_a is the activation energy for crystallization calculated by using

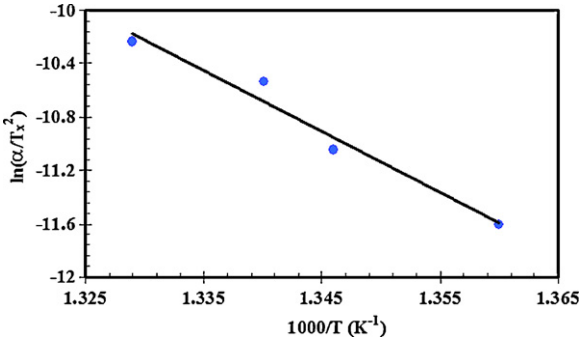

Fig. 2. Kissinger plot for crystallization of the Bi-3223 sample prepared.

equation (1) and R is the gas constant. The Avrami parameter, n, was calculated to be 2.9 ± 0.3 which is in agreement with the one of [47]. The result indicates that the growth is diffusion-controlled and simultaneous nucleation with three-dimensional parabolic growth takes place in the system during the crystallization process [48]. For the diffusion-controlled growth, $1.5 < n < 2.5$ reflects growth of small particles with a decreasing nucleation rate [49]. However, if $n > 2.5$, small particles grow with increased nucleation rate. Increase of the nucleation rate results in the compositional fluctuations in the regions adjacent to the growing nuclei.

Fig. 3a shows TG and DTA patterns at the heating rate of 10 °C min^{-1} in the same figure. In TG pattern, mass gain started at 357 °C, reached a maximum level at 677 °C and after 772 °C, the loss in mass started. The mass gain between 357 and 677 °C was calculated to be 0.093 mg.

BSCCO based superconducting system shows high oxygen sensitivity and oxygen atoms incorporate to its unit cell during superconducting phase formation. Activation energy for oxygen diffusion can be calculated by equation given by [50]:

$$\ln\left[\ln\left(\frac{m}{m_0}\right)\right] = -\frac{E}{R}\left(\frac{1}{T}\right) + \text{Constant} \quad (3)$$

where E is the activation energy for oxygen diffusion, m is the mass of material at certain temperature, m_0 is the starting mass, T is the temperature and R is the ideal gas constant. $\ln[\ln(m/m_0)]$ vs $1/T$ plot is given in Fig. 3b. Slope of the curve gives activation energy for oxygen diffusion, E. Two different energy values were obtained in two different temperature regions, Fig. 3b and Table 3.

As mentioned above, TG analysis is related to mass loss and/or gain with temperature due to oxygen out and/or diffusion. Two different slopes in the plot of $\ln[\ln(m/m_0)]$ vs $1/T$ were obtained, Fig. 3b. The BSCCO HT_c superconducting system has oxygen deficiencies in its unit cell which must be filled by oxygen ions for superconductivity. During heat treatment, oxygen ions rapidly diffuse to the system up to a certain temperature and then diffusion rate decreases due to oxygen saturation of the system. In the present study, E was calculated to be 8.6 kJ mol^{-1} between 370 and 580 °C and 4.4 kJ mol^{-1} above 580 °C. At low temperatures, rapid oxygen diffusion to the system takes place to fill the oxygen deficiencies, which means high activation energy for diffusion. However, since the number of oxygen deficiencies reduces with increasing temperature, less number of oxygen ions diffuse into the system, which means low activation energy.

In this work, any whisker growth was not observed at 790–805 °C and above 860 °C but in the range of 810 and 850 °C, whiskers in different sizes were observed. The longest whiskers were obtained under heat treatment condition of 850 °C–120 h, Table 1. This temperature corresponds to partially melting temperature in DTA pattern and the mass loss temperature in TG pattern, Fig. 3a. Therefore, it is obvious that whiskers with maximum length have grown in the temperature region at which oxygen loss rate is high and partially melting occurs. The results obtained indicated that the Bi-2212 whiskers grow on the partially melted main matrix. The growth of whiskers on the partially melted matrix supports two different growth mechanisms: "bouncy effect mechanism" proposed by Cecchetti et al. [51], which is a theoretical model, and "microcrucible mechanism" by Matsubara and Yamashita [52].

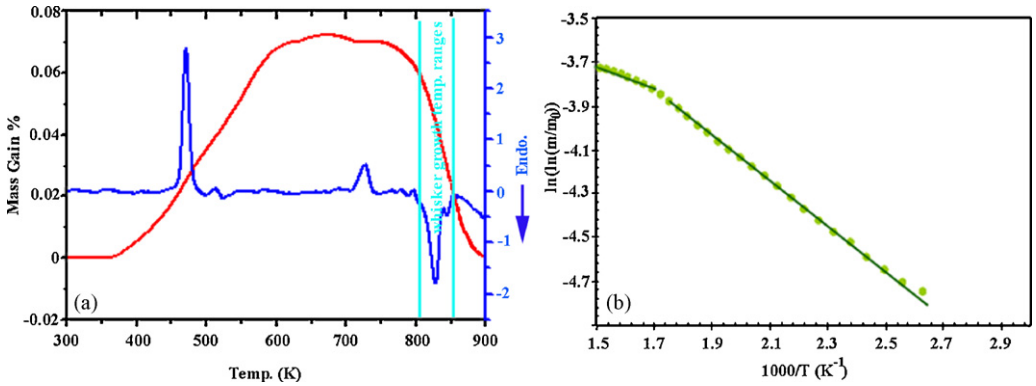

Fig. 3. (a) TG and DTA curves of the material heated 10 °C min^{-1} and (b) ln[ln(m/m_0)] vs 1000/T plot.

Table 3
TG data and activation energies for oxygen diffusion.

Material	Δm (mg)	T_{onset} (°C)	T_{finish} (°C)	ΔT (°C)	E_1 (kJ mol^{-1})370–580 °C	E_2 (kJ mol^{-1})580–660 °C
Bi-3223	0.093	357	677	320	8.6	4.4

In bouncy effect mechanism, it is assumed that needle-like crystals are oriented along c-axis due to interactions among grains in the temperature region in which solid and liquid phases exist together (peritectic phase). At the peritectic phase, BSCCO crystals are rather mobile, facilitating their contact and interaction with each other. This interaction leads to a-(b-) axis crystal growth easier than c-axis growth and grains can easily growth needle-like shape in the partial melting temperature zone on the material. This means that while the crystal growth is along a-(b-) direction, the grain orientation along c-direction.

The growth of whiskers on the partially melted matrix is also strongly evidence for the "microcrucible mechanism" proposed by Matsubara and Yamashita [52]. According to this model, the Bi-2212 whisker and the surrounded liquid phase are supported by the rigid skeleton of the Bi–Sr–Ca–Al–O complex oxide, which produces the growth of the whiskers by pushing up from the surface to out side of the matrix. The supplementation of the source materials to the melt at the bottom part of the whisker appears to proceed through diffusion of ions in the matrix.

3.2. XRD results

XRD patterns of glass and materials heat treated at 500, 600, 700, 800 °C for 120 h and whiskers fabricated at 850 °C, respectively, are shown in Fig. 4. The XRD pattern of the glass material showed a broad halo at around $2\theta \cong 30^\circ$. This clearly indicates that the material was found to be fully in the glass form and the absence of long-range atomic arrangement and periodicity of three-dimensional network in the BSCCO glass material prepared.

Crystallization in the material heat treated at 500 °C for 120 h started and the Bi-2201 superconducting phase with $Sr_3Bi_2Cu_2O_x$ and $(Sr,Ca)_{12}Cu_{24}AlO_x$ phases were detected. When the material was heat treated at 600 and 700 °C for 120 h, Bi-2201 and $Bi_2Ca_{0.5}Sr_{2.5}Cu_3O_x$ phases with $(Sr,Ca)_{12}Cu_{24}AlO_x$ were obtained. In the case of heat treatment at 800 °C for 120 h, the Bi-2212 superconducting phase was formed and secondary phases such as $Bi_2Ca_{0.5}Sr_{2.5}Cu_3O_x$ and $(Sr,Ca)_{12}Cu_{24}AlO_x$ were also detected.

Whiskers grown on the glass precursor heat treated at 850 °C for 120 h which is the optimum heat treatment condition for the whisker growth in our experiments consisted of only Bi-2212 phase without any impurity phases. Only c-axis oriented sharp (0 0 l) peaks were obtained. This strongly showed that the crystal orientation in the whiskers fabricated is along the c-axis. It was also found that whisker has tetragonal symmetry and the unit-cell parameters were calculated to be $a(=b) = 5.41$ Å and $c = 30.62$ Å which are close to that of previously obtained values [53,54].

3.3. SEM investigations

As mentioned in the DTA results, the n value obtained in this work is 2.9 ± 0.3. This value is higher than 2.5 and indicates the diffusion-controlled growth mechanism of small nucleation centers with increasing nucleation and growth rate by increasing the heat treatment temperature. The evidence of this type of growth is obtained on the surface of the glass materials when they were heated up to ~500 °C for 120 h, Fig. 5a. It was observed that small particles grown on surface of the material, which act as a nucleation centres. From EDX results, atomic concentration of ~500 nm sized nucleation centres was found to be Bi-1.8 at%, Sr-26.1 at%, Ca-32.5 at%, Cu-0.6 at% and Al-39 at% (where Al comes from the crucible used during melting and heat treatment) and the main glass matrix has $Bi_{2.8}Sr_2Ca_{0.6}Cu_2Al_{0.3}O_x$. This suggests a significant

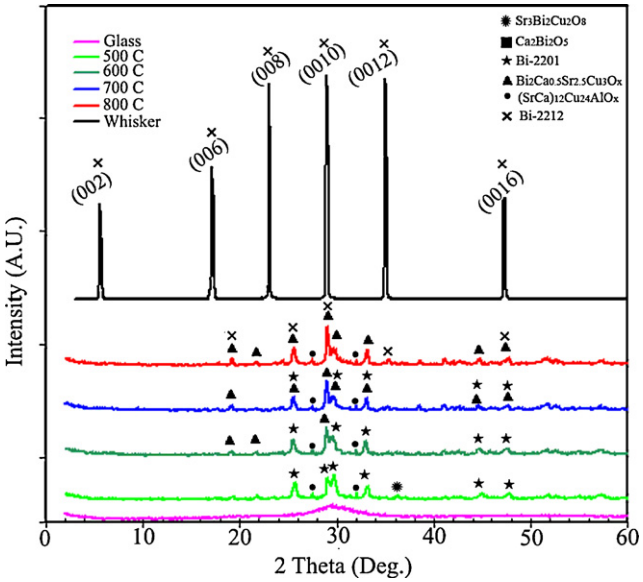

Fig. 4. XRD patterns of glass, materials heat treated at different temperatures and whiskers fabricated at 850 °C for 120 h.

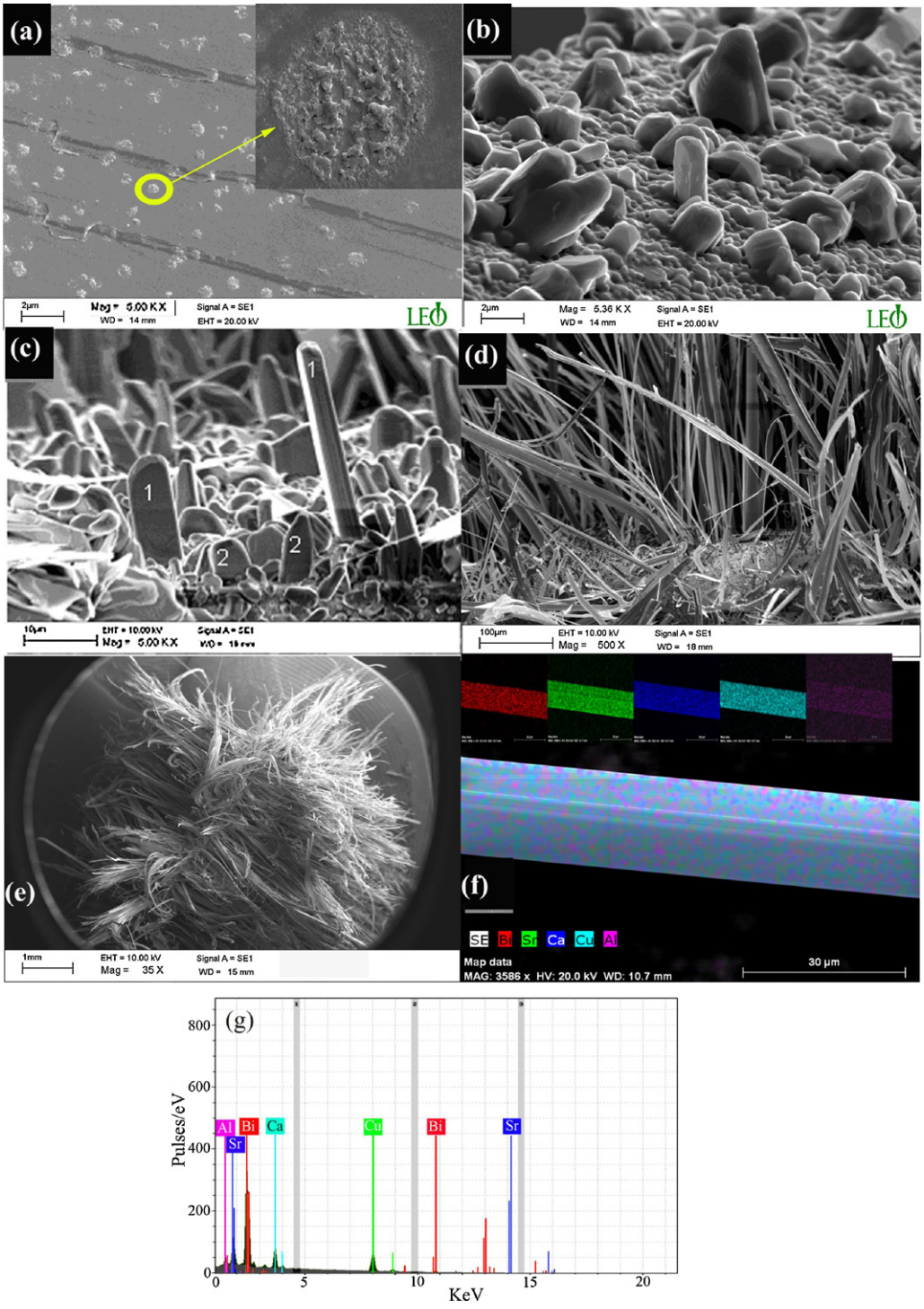

Fig. 5. SEM micrographs of (a) first nucleation centers at 500 °C for 120 h, (b) nucleation centers at 800 °C for 120 h, (c) first whiskers fabricated at 810 °C for 120 h, (d) the whiskers fabricated at 820 °C for 120 h, (e) long whiskers fabricated at 850 °C for 120 h, (f) dot mapping analysis of whisker fabricated at 850 °C for 120 h and (g) EDX pattern of whisker fabricated at 850 °C for 120 h.

compositional fluctuation between the nucleation centres and main matrix. High Al ratio on the nucleation centre supports the microcrucible mechanism for whisker growth [55].

An increase on the heating temperature to 800 °C for 120 h causes a chain reaction-like process leading to an increase on the nucleation and crystal growth rates. There has been evidence that the growth of the whiskers starts directly on these nucleation centres and grows continuously with temperature and time, Fig. 5b. The composition of small whisker-like phase, Fig. 5b, is obtained to be $Bi_3(SrCa)Cu_2O_x$ (except Al contaminations which is less than 0.7%).

Fig. 5c shows surface of the glass material heat treated at 810 °C for 120 h. The size and the quantity of the whiskers increased significantly compared to small crystals grown at the 800 °C. The compositions of the crystals were also found different. The long column/whisker-like crystals (denoted as 1 in Fig. 5c) were found to have slightly Bi-rich Bi-2212 phase. The composition of the small crystals (denotes as 2) was found to be $Bi_2(SrCa)Cu_2O_x$ phase.

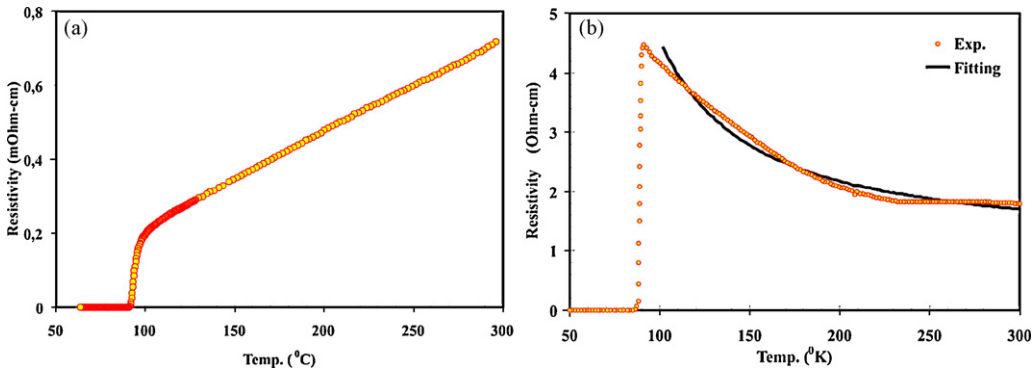

Fig. 6. Temperature dependence of (a) in-plane resistivity and (b) out-of-plane resistivity.

When the temperature was increased to 820 °C for a 120 h period, significant amount of whiskers was found to grow on the surface, Fig. 5d. The grown whiskers have smooth surface and their maximum length reached to 12 mm with 5–20 μm of width and their thickness was less than 1 μm. The composition of these whiskers was found to be Bi-2212 without any impurity phases, except very small amount of Al (0.6% atomic concentration). Although smaller, 3–5 mm, and thinner, 0.5–1 μm, whiskers were grown under heat treatment conditions between 20–120 h at 820 °C, the numbers of these whiskers, however, were very few compared to that of at 240 h. However, no significant changes were found on the size and numbers of the whiskers when the treatment time was expanded to 300 h at 820 °C.

The best whisker formation was obtained under 850 °C at 120 h. The length of the whiskers reached to 18 mm, while a thickness of 700 nm – 1 μm and width of 5–60 μm was observed, Fig. 5e. The SEM observations have revealed a continuous and very smooth surface formation with no grain boundaries on the direction of the growth. Any impurity (but Al which diffuses into the sample from the Al_2O_3 boats during the heat treatment) or substructures were not observed and the composition of the whiskers perfectly fits the Bi-2212 phase including small ratio of Al (0.5–0.9%). This result indicates a clear and perfect microstructural formation as seen in Fig. 5f. The EDX pattern of the whisker is shown in Fig. 5g. The stoichiometric composition of whiskers obtained is presented in Table 1. Results are agreement with the results by Matsubara et al. [52,55]

The whiskers obtained at 850 °C with long heating times (>120 h) showed no improvement on the microstructure, sizes and the numbers. Even partly melted surface or randomly grown multiphase whiskers were obtained during long time heat treatment (>280 h).

3.4. Resistivity results

Temperature dependence of the in-plane, ρ_{ab}, and out-of-plane, ρ_c, resistivity of whiskers are shown in Fig. 6a and b, respectively. The in-plane resistivity, ρ_{ab}, exhibited almost linear temperature dependence from room temperature to near T_c (94.8 K), Fig. 6a, suggesting regular metallic structure and the electron–phonon scattering is dominant in this temperature range.

The out-of-plane resistivity passing through a local minimum value attain a maximum ($d\rho_c/dT < 0$) and then fall, vanishing below T_c (92.3 K), Fig. 6b. This type of the out-of-plane resistivity behavior is attributed to the semiconducting arrangement of planes along the c-axis in the BSCCO system. The metallic Cu–O planes are responsible for the in-plane conductivity, while tunnelling of the charge carriers between the semiconducting Bi–O planes along the c-axis contributes to the out-of-plane conductivity. The sharp fall in ρ_c at T_c interrupts the rise corresponding to the semiconducting charge-ordering state. Between 200 K and room temperature, however, this became almost linear, Fig. 6b. This is obviously a typical result indicating the anisotropic nature of this material for Bi-2212 single crystal samples [56].

The temperature dependence of the out-of-plane resistivity fits the Arhenius type relation;

$$\rho_c(T) = \rho_0 e^{\Delta E/k_B T} \quad (4)$$

where ρ_0 is the pre-exponent factor, ΔE is the semiconducting energy band gap, k_B is the Boltzmann constant [60]. Fitting curve is shown in Fig. 6b with black solid line. Fitting parameters ρ_0 and ΔE were found to be 1.04 ± 0.002 and 12.7 ± 0.03 meV which are good agreement with previous studies in the literature [57].

For the Bi-2212 whisker, we can calculate hole concentration per Cu atom using equation given by Presland et al. [58]:

$$T_c/T_c^{\max} = 1 - 82.6[p - 0.16]^2 \quad (5)$$

where $T_c^{\max}$ is taken 95 K for the Bi-2212 system and p the number of the holes per Cu. This equation was used to the doped/substituted BSCCO system previously by many groups [59,60]. Calculations for the Bi-2212 system show that the p-value ranges between 0.16 and 0.22 [60]. However, the computed values of p in this work are 0.165. This value suggests that the hole concentration of the whiskers obtained was found in optimally doped ranges.

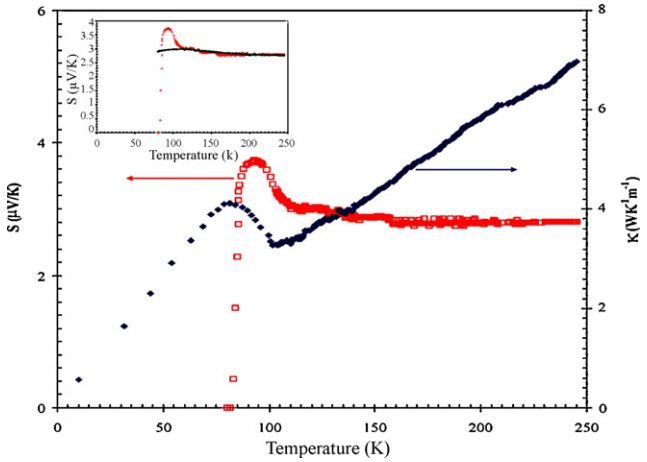

Fig. 7. Temperature dependence of thermoelectric power, $S(T)$, and thermal conductivity, $\kappa(T)$, for single crystal Bi-2212 whisker.

3.5. Thermoelectric power (TEP) results

Fig. 7 shows the temperature dependence of thermoelectric power data, $S(T)$, for the whisker. The $S(T)$ value over the measurement temperatures was found to be positive over all temperature region. Similar behavior was obtained in different BSCCO systems [61–66,26,21]. Room temperature S values indicate optimally doping state for whiskers [61]. With decreasing temperature the magnitude of S increased slowly down to a temperature of ~110 K. S increased sharply near 90 K, signifying the occurrence of superconductivity. With further decrease of temperature, S passed through a maximum and then drop to zero at 83 K, suggesting that S vanishes at the superconducting state.

Several models have been proposed to analyze the thermoelectric power data of the HT_c materials. As discussed in the out-of-plane resistivity investigation, the HT_c BSCCO system consists mainly of the Bi–O and Cu–O plane which are responsible for transport in the BSCCO system. The other planes, Sr–O and Ca–O behave as charge reservoir blocks (CRB). Therefore, a model based on two-band approximation is suitable to analyze the TEP data of the BSCCO whisker prepared; *Two band model with linear T-term*. Since other models were developed with respect to one-band approximation, we have not preferred for TEP analysis.

3.5.1. Two band model with linear T-term

The thermoelectric power results of the HT_c systems show a similarity close to the thermoelectric power results of mixed valent heavy fermion systems such as $CeNi_x$. The formula for these compounds was proposed by Gottwick et al. assuming a Lorenzian resonance near the Fermi level [67] in the form:

$$S = \frac{AT}{B^2 + T^2} \tag{6}$$

and

$$A = 2\frac{E_0 - E_F}{e} \qquad B = 3\frac{[E_0 - E_F]^2 + \Gamma^2}{\pi^2 k_B^2} \tag{7}$$

where E_0 is the center of the resonance and Γ is the width of resonance. The theory is based on a superposition of a broad band and narrow band in the density of state. The narrow band has the width Γ and positioned at E_0 close to the Fermi energy, E_F. Forro et al. added a linear term to Eq. (6) to fit the HT_c Bi-2212 single crystals [68]:

$$S = \frac{AT}{B^2 + T^2} + \alpha T \tag{8}$$

where αT term presents the normal band contribution. It is worth noting that the temperature region very close to T_c was not considered in these analyses due to the possible superconducting fluctuations. The best fit of Eq. (8) to the $S(T)$ data is shown in Fig. 7-inset. The experimental data fitted well with Eq. (8). The fitting parameters were obtained to be $A = 437.79\ \mu V$, $B = 86.58$ K, $\alpha = 4.776 \times 10^{-3}\ \mu V\,K^{-2}$, $E_0 - E_F = 2.54$ K and $\Gamma = 156.95$ K, respectively. The reasonable fitting values were found, compared to previous values obtained for the Bi-2212 system [26].

3.6. Thermal conductivity, κ(T), results

Temperature dependence of thermal conductivity for the fabricated whiskers is shown in Fig. 7. For $T > T_c$, $\kappa(T)$ decreased linearly with decreasing temperature. A peak was observed just below T_c in $\kappa(T)$. Similar behavior was observed in the a-axis κ(T) of the Pb-doped Bi-2212 whisker fabricated by Verebely et al. [69,28] and also for single crystal Bi-2212 by Ando [70]; in the studies, a peak in κ was obtained just below T_c. However, in another study by Verebely et al., different results were found for Bi-based whiskers including Ni, Fe and Co [28,71]. They reported a strong upturn in κ between 10 and 30 K. Variations in κ was ascribed to changes of electronic structure due to the magnetic substitutional elements. In addition, it was believed that a sharp increase in κ between 10 and 30 K was due to incomplete condensation of carriers.

For the peak observed in thermal conductivity just below T_c two scenarios have been proposed: one attributes it to decrease in scattering of phonons by carriers due to condensation of electrons into Cooper pairs and so the increase of phonon mean free path [72]. The other attributes it to a decrease in quasi-particle scattering below T_c and so an increase in the quasi-particle mean free path [73]. Recent experimental and theoretical studies showed that the peak in $\kappa(T)$ has an electronic origin [28,70–73]. Therefore, we believed that the peak is due to the suppressed quasi-particle scattering rate in the superconducting state.

4. Conclusion

Bi-2212 superconducting whiskers have been fabricated successfully by using glass precursors. Thermal, structural/microstructural and transport properties were characterized. The XRD and SEM investigations showed a highly c-axis orientation and a single crystal formation without any grain boundaries.

The in-plane resistivity, ρ_{ab}, showed linear temperature dependence between 300 and 94.8 K (~T_c). The out-of-plane resistivity increased as temperature decreased attained a maximum and then dropped to zero at 92.3 K which is near T_c. This type behavior is attributed to tunnelling of the charge carriers between the semiconducting Bi–O planes along the c-axis.

$S(T)$ is obtained to be positive, indicating that major charge carriers are holes. The magnitude of S was found to increase with decreasing temperature, reaching a maximum value around T_c. With reducing temperature further, the thermoelectric power is found to fall rapidly to zero, signifying the occurrence of superconductivity. "*Two band model with linear T-term*" was used to analyze the TEP data. The rapid rise of κ just below T_c indicates the enhancement of the quasi-particle contribution to the heat conductivity and so increase of the quasi-particle mean free path. It supports an increase on the electrical contribution to the total thermal conductivity below T_c.

References

[1] K. Kadowaki, H. Yamaguchi, K. Kawamata, T. Yamamoto, H. Minami, I. Kakeya, U. Welp, L. Ozyuzer, A. Koshelev, C. Kurter, K.E. Gray, W.-K. Kwok, Phys. C 468 (2008) 634–639.
[2] I. Kakeya, K. Fukui, K. Kawamata, T. Yamamoto, K. Kadowaki, Phys. C 468 (2008) 669–673.
[3] V.A. Yampol'skii, D.R. Gulevich, S. Savel'ev, F. Nori, Phys. Rev. B 78 (2008) 054502.
[4] S. Okano, A. Irie, G. Oya, J. Korean Phys. Soc. 48 (5) (2006) 1080–1083.
[5] M. Schmidt, H.-J. Krause, M. Banzet, D. Lomparski, J. Schubert, W. Zander, Y. Zhang, R. Arkam, M. Fardmanesh, Supercond. Sci. Technol. 19 (2006) S261–S265.
[6] A. Krapf, G. Lacayo, G. Kastner, W. Kraak, N. Pruss, H. Thiele, H. Dwelk, R. Herrman, Supercond. Sci. Technol. 4 (1991) 237.
[7] S.-Y. Oh, S.-J. Kim, G.-S. Kim, M. Nagao, T. Hatano, Phys. C 445–448 (2006) 459–461.
[8] M. Tange, T. Amano, M. Yokoshima, S. Nishizaki, R. Yoshizaki, Phys. C 412–414 (2004) 610–613.
[9] R. Jayavel, T. Mochiku, S. Ooi, K. Hirata, Phys. C 378–381 (2002) 118–121.
[10] P. Badica, K. Togano, A. Awaji, K. Watanabe, H. Kumakura, Supercond. Sci. Technol. 19 (2006) R81.
[11] S. Altin, M.A. Aksan, Y. Balci, M.E. Yakinci, J. Supercond. Nov. Magn. 22 (2009) 775–784.
[12] T.E. Oskina, Ya.G. Ponomarev, H. Piel, Yu.D. Tretyakov, B. Lehdorff, Phys. C 266 (1996) 115–126.
[13] I. Matsubara, H. Kageyama, H. Tanigawa, T. Ogura, H. Yamashita, T. Kawai, Jpn. J. Appl. Phys. 28 (1989) L1121.
[14] S. Kishida, H. Uemoto, J. Mod. Phys. B 16 (2002) 4497.
[15] J. Jung, J.P. Franck, D.F. Mitchell, H. Claus, Phys. C 156 (1988) 494–496.
[16] M. Nagao, M. Sato, H. Maeda, S. Kim, T. Yamashita, Jpn. J. Appl. Phys. 41 (2002) L43–L45.

[17] M. Yamada, N. Hosi, S. Kambe, Phys. C 378–381 (2002) 152–154.
[18] H. Jin, S. Skwirblies, J. Kotzler, J. Cryst. Growth 207 (1999) 154–159.
[19] S. Altin, M.A. Aksan, Y. Balci, M.E. Yakinci, Mater. Sci. Technol. in press, http://www.ingentaconnect.com/content/maney/mst/pre-prints/mst8842.
[20] H. Uemoto, M. Mizutani, S. Kishida, T. Yamashita, Phys. C 392–396 (2003) 512.
[21] M.A. Aksan, M.E. Yakinci, J. Mater. Process. Technol. 196 (2008) 365–372.
[22] C. Sun, H.S. Yang, L. Cheng, J.B. Wang, X.Y. Xu, S.Q. Ke, L.Z. Cao, Phys. Rev. B 78 (2008) 104518.
[23] R. Awad, Al Abou-Aly, S. Isber, W. Malaeb, Solid State Commun. 145 (2008) 201–206.
[24] S.H. Naqib, Supercond. Sci. Technol. 20 (2007) 964–968.
[25] M.A. Aksan, M.E. Yakinci, J. Alloy Compd. 433 (2007) 22–32.
[26] D.R. Sita, R. Singh, Phys. C 296 (1998) 21–28.
[27] F. Chen, K.L. Stokes, R. Funahashi, Appl. Phys. Lett. 81 (2002) 2379–2381.
[28] D.T. Verebelyi, C.W. Schneider, Y.K. Kuo, M.J. Skove, G.X. Tessema, J.E. Payne, Phys. C 328 (1999) 53–59.
[29] M.A. Aksan, S. Altin, Y. Balci, M.E. Yakinci, Mater. Chem. Phys. 106 (2007) 428–436.
[30] M. Matsukawa, H. Noto, A. Tamura, H. Furusawa, X. Yao, S. Nimori, N. Kobayashi, Y. Shiohara, Supercond. Sci. Technol. 19 (2006) 777–782.
[31] H. Fujishiro, S. Nariki, M. Murakami, Supercond. Sci. Technol. 19 (2006) S447–S450.
[32] J. Zhao, C.X. Shen, F. Zhou, J.W. Xiong, L.H. Liu, Z.X. Zhao, Supercond. Sci. Technol. 18 (2005) 966–969.
[33] I.H. Gul, M. Anis-ur-Rehman, A. Maqsood, Phys. C 450 (2006) 83–87.
[34] C. Uher, W.N. Huang, Phys. Rev. B 40 (1989) 2694–2697.
[35] R.C. Yu, M.B. Salamon, J.P. Lu, W.C. Lee, Phys. Rev. Lett. 69 (1992) 1431–1434.
[36] K. Krishana, J.M. Harris, N.P. Ong, Phys. Rev. Lett. 75 (1995) 3529–3532.
[37] P.J. Hirschfeld, W.O. Putikka, Phys. Rev. Lett. 77 (1996) 3909–3912.
[38] J.L. Cohn, M.S. Osofsky, J.L. Peng, Z.Y. Li, R.L. Greene, Phys. Rev. B 46 (1992) 12053–12056.
[39] S. Aukkaravittayapuni, K.A. Benedict, I.G. Gorlovat, P.J. Kingt, Yu I. Latyshevt, C. Staddont, S.G. Zybtsevt, Supercond. Sci. Technol. 8 (1995) 718–725.
[40] M.A. Aksan, M.E. Yakinci, Y. Balci, J. Therm. Anal. Calorim. 81 (2005) 417–423.
[41] M.A. Aksan, M.E. Yakinci, J. Alloy Compd. 385 (2004) 33–43.
[42] H.E. Kissinger, J. Res. Natl. Bur. Stand. 57 (1956) 217.
[43] K. Matusita, S. Sakka, Phys. Chem. Glasses 20 (1979) 81.
[44] M. Avrami, J. Chem. Phys. 7 (1939) 1103.
[45] M.R. De Guire, N.P. Bansal, C.J. Kim, J. Am. Ceram. Soc. 73 (1990) 1165–1171.
[46] M.E. Yakinci, I. Aksoy, A. Ozdes, Phys. C 235–240 (1994) 959–960.
[47] D.P. Matheis, S.T. Misture, R.L. Snyder, Phys. C 207 (1993) 134–142.
[48] A. Karamanov, M. Pelino, J. Non-Cryst. Solids 290 (2001) 173–179.
[49] Z.J. Yan, S.R. He, J.R. Li, Y.H. Zhou, J. Alloy Compd. 368 (2004) 175–179.
[50] A. Broido, J. Polym. Sci. Part A-2 7 (1969) 1761.
[51] E. Cecchetti, P.J. Ferreira, J.B. Vander Sande, Supercond. Sci. Technol. 13 (2000) 1270–1278.
[52] I. Matsubara, H. Yamashita, J. Cryst. Growth 128 (1993) 719.
[53] J. Jung, J.P. Franck, S.C. Cheng, S.S. Sheinin, Jpn. J. Appl. Phys. 28 (1989) L1182.
[54] H. Jin, Z. Hu, Y. Ge, S. Lin, Q. Liu, C. Shi, Phys. C 197 (1992) 315.
[55] I. Matsubara, R. Funashi, T. Ogura, H. Yamashita, K. Tsuru, T. Kawai, J. Cryst. Growth 141 (1994) 131.
[56] G. Balestrino, E. Milani, C. Aruta, A. Varlamov, Phys. Rev. B 54 (1996) 3628–3632.
[57] C. Boulesteix, Y. Marietti, T. Badeche, H. Tatarenko-Zapolsky, V. Grachev, O. Monnereau, H. Faqir, G. Vacquier, J. Phys. Chem. Solids 61 (2000) 585–592.
[58] M.R. Presland, J.L. Tallon, R.G. Buckley, R.S. Liu, N.E. Floer, Phys. C 176 (1991) 95–105.
[59] C. Terzioglu, M. Yilmazlar, O. Ozturk, E. Yanmaz, Phys. C 423 (2005) 119–126.
[60] C. Terzioglu, H. Aydin, O. Ozturk, E. Bekiroglu, I. Belenli, Phys. B 403 (2008) 3354–3359.
[61] S.D. Obertelli, J.R. Cooper, J.L. Tallon, Phys. Rev. B 46 (1992) 14928.
[62] V.P.S. Awana, R. Lal, A.V. Narlikar, J. Phys.: Condens. Matter 7 (1995) L171–L174.
[63] S. Chatterjee, P.K. Pal, S. Bhattacharya, B.K. Chaudhuri, Phys. Rev. B 58 (1998) 12427–12432.
[64] M.M. Ibrahim, S.M. Khalil, A.M. Ahmed, J. Phys. Chem. Solids 61 (2000) 1553–1560.
[65] V.P.S. Awana, V.N. Moorty, A.V. Narlikar, Phys. Rev. B 49 (1994) 6385–6387.
[66] R. Singh, D.R. Sita, Phys. C 312 (1999) 289–298.
[67] U. Gottwick, K. Gloss, S. Horn, F. Steglich, N. Grewe, J. Magn. Magn. Mater. 47–48 (1985) 536–538.
[68] L. Forro, M. Raki, J.Y. Henry, C. Ayache, Solid State Commun. 69 (1989) 1097–1101.
[69] http://proquest.umi.com/pqdweb/?index=1&did=737989771&SrchMode=1&sid=3&Fmt=2&VInst=PROD&VType=PQD&RQT=309&VName=PQD&TS=1273564036&clientId=46703.
[70] Y. Ando, J. Takeya, Y. Abe, K. Nakamura, A. Kapitulnik, Phys. Rev. B 62 (2000) 626–630.
[71] V. Gusakov, A. Jezowski, S. Barilo, M. Kalanda, A. Saiko, Phys. B 284–288 (2000) 989–990.
[72] M. Matsukawa, T. Mizukoshi, K. Noto, Y. Shiohara, Phys. Rev. B 53 (1996) R6034–R6037.
[73] M. Ausloos, M. Houssa, Supercond. Sci. Technol. 12 (1999) R103–R114.